Journal Name

Dynamic Article Links ►

Cite this: DOI: 10.1039/c0xx00000x

www.rsc.org/xxxxxx

ARTICLE TYPE

Magnetorheological brush – a soft structure with highly tuneable stiffness

Xiao Huang,[a,b] Akshi Mohla,[c] Wei Hong,*[c,b] Ashraf F. Bastawros[c] and Xi-Qiao Feng [a]

Received (in XXX, XXX) Xth XXXXXXXXX 20XX, Accepted Xth XXXXXXXXX 20XX

DOI: 10.1039/b000000x

By combining the field-stiffening effect of magnetorheological (MR) elastomers and the Euler buckling mechanism, we developed a brush-like magneto-active structure with highly tuneable stiffness. When the applied mechanical load is within a certain range, the effective stiffness of the structure can be tuned by several orders of magnitude with the applied magnetic field. The performance of the structure and its dependence on various synthesis parameters, such as the curing field and filler concentration, were investigated experimentally. It is found that the increase in the critical load for buckling is more than the contribution from the stiffening of the MR elastomer. To unravel the relation between the stiffness increase and the applied field, a theoretical model with coupled mechanical deformation and magnetic field is established. The prediction of the model agrees well with experimental results. The theory may also be used to model the behaviour of other similar materials, such as MR gels. The MR brush developed in this research hold promise for potential applications in smart structures or devices that require mechanical stiffness to be tuneable in a relatively large range. As the amplification mechanism is independent of the base material, it could be used in conjunction with emerging MR materials for further enhanced performance.

1. Introduction

Magnetorheological (MR) materials, including MR fluids, MR elastomers and MR gels, are an important group of smart materials whose rheological properties can be varied rapidly and in most cases reversibly by applying a magnetic field.[1-5] MR materials are typically comprised of micron-sized magnetic particles suspended in a non-magnetic matrix. For example, MR fluids are liquid suspensions of magnetic particles. With their yield stresses and viscosities tuneable by two to three orders of magnitude under applied magnetic field,[6] MR fluids have found applications in brakes,[7] dampers,[8] isolators,[9] etc. One major shortcoming of most MR fluids is the settling of particles.[5,10] With the fluid component replaced by a soft polymer, MR elastomers are solid analogues of MR fluids. Depending on synthesis processes, the magnetic filler particles may disperse randomly or form aligned chains, resulting in isotropic or anisotropic MR elastomers, respectively.[2,11,12] The microstructural parameters, such as the size, alignment, and composition of the filler, have significant influences on the MR effect.[13-17] Using solids as substrate, the sedimentation problem is circumvented in MR elastomers at a cost of the tuneable range of the rheological properties. The reported relative change in the effective elastic modulus of MR elastomers is less than 100%,[11] much lower than that of MR fluids. One way of increasing the relative change of stiffness is to use a softer material as the matrix. Significant progress has been made recently by using highly swollen polymeric gels as matrices.[18,19] Just like in MR fluids, the introduction of liquid solvent and other very soft materials may also limit the stability and durability of the products.

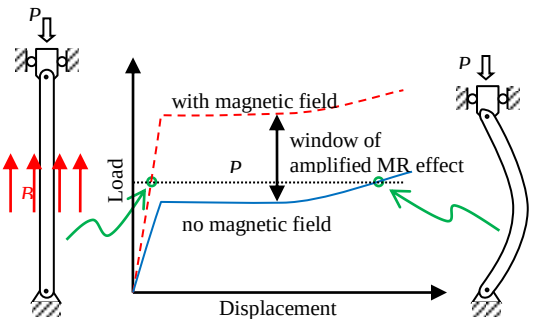

Fig. 1 MR-elastomer column under axial compression. When the load is between the critical value with a magnetic field and that without magnetic field, the responses of the column differ drastically in these two scenarios.

This paper reports an MR structure that enhances the performance of solid MR elastomers by combining the MR effect with the buckling instability. The principal working mechanism of the structure is illustrated in Fig. 1. Consider an elastic column under uniaxial compression. Elementary mechanics suggests that when the load exceeds the critical value, $P_c = \pi^2 EI/L^2$ with EI being the bending stiffness and L the length, the column will

buckle and exhibit a much larger end-to-end deformation. Now imagine that the column is made of an MR elastomer with bending stiffness dependent on the applied field. If, for example, the load is applied within the window between the critical forces of the cases with and without a magnetic field, the corresponding deformations can be very different, as sketched in Fig. 1. The effective compressive stiffness of the column is thus changed greatly by the magnetic field. Comprised of an array of MR columns (the bristles) grown on a flat substrate, the MR brush structure reported in this paper utilizes such a mechanism, although the details may differ from the simple buckling of an Euler beam.

The performance of a typical MR brush sample is demonstrated in Fig. 2. In the absence of a magnetic field, the thin bristles were prone to buckling under a very low force. For the sample shown in Fig. 2, a compressive load of 0.1 kgf was enough to collapse the entire structure, giving an overall compressive strain of ~70%. When brought to the proximity of a permanent magnet (~0.4 T), the bristles were stiffened, and the critical load increased. No buckling took place even under a higher load (0.2 kgf), and the deformation was very small (compressive strain ~5%). From the difference in deformation, we can estimate the increase in the effective stiffness under the magnetic field to be at least one order of magnitude.

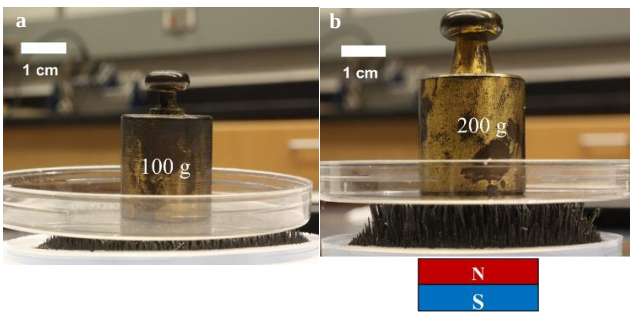

Fig. 2 Demonstration of the highly tunable stiffness of an MR brush. (a) In the absence of magnetic field, the columns buckled and the structure collapsed with large deformation under a load of 0.1 kgf. (b) Under a magnetic field, the same structure did not buckle and showed little deformation even under a load of 0.2 kgf.

While a detailed model for the working mechanism will be introduced in Section 2, the MR structure may be regarded as a solid analogue of the MR fluid by replacing the liquid carrier with air. The columnar structure resembles the ailgned particle chains in an MR fluid when brought into a magnetic field. The resulting MR brush has highly tuneable stiffness just as an MR fluid, but its all-solid structure is much more stable than the latter. Therefore, it can be a great alternative to MF fluids in applications where better stability or durability is needed.

2. Theory

As will be shown by the experimental results in later sections, the increase of the buckling stress of an MR-brush bristle is more than the contribution from the field-induced modulus increase. This amplification effect can be understood from the coupling between the magnetic field and the large deformation of the structure. The buckling of an elastic column reduces the potential energy of a load, at the expense of a smaller elastic energy from bending. At the same time, if the column is made of more permeable material than air, the buckled geometry will also perturb the original close-to-uniform magnetic field. In general, such a perturbation increases the magnetic energy in the system. As a result, the buckling is energetically more difficult. In other words, the critical load is higher than that predicted by Euler buckling considering only the modulus change.

To quantitatively characterize this mechanism, a simple theoretical model will be formulated in this section. Consider a representative column (a bristle) in an MR brush, as sketched in Fig. 3. The entire structure is much larger than this column, so that the edge effect could be neglected. Here, we will only consider the case when both ends of the column are clamped. The cases of other boundary conditions can be analyzed similarly, and the results will differ by a numerical factor, but the physics shall not be altered. Under the prescribed boundary conditions, the wavelength of the lowest order buckling mode is just the length of the column, L. For the purpose of predicting the onset of instability, it is assumed that the amplitude of deflection is much smaller than the wavelength, $A \ll L$, and the deflection function can be assumed to be in a sinusoidal form, $w = A\left(1-\cos\frac{2\pi x}{L}\right)$.

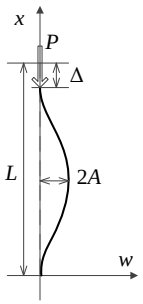

Fig. 3 Schematic drawing of a single column in the MR-brush structure.

The elastic energy from bending the column reads

$$U_b = \int_0^L \frac{1}{2} EIw''^2 \mathrm{d}x = 4\pi^4 EI \frac{A^2}{L^3} \tag{1}$$

Here, the prime operator indicates a derivative with respect to coordinate x : $w' = \mathrm{d}w/\mathrm{d}x$, and the double prime indicates a second order derivative. Due to buckling, the end-to-end distance of the column is shortened by

$$\Delta = \int_0^L \frac{1}{2}(w')^2 \mathrm{d}x = \pi^2 \frac{A^2}{L}. \tag{2}$$

In the absence of a magnetic field, the total potential energy of the system, including the elastic energy and the potential of the axial load P can be calculated as

$$U = U_b - P\Delta = \pi^2 \frac{A^2}{L}\left(4EI\frac{\pi^2}{L^2} - P\right). \tag{3}$$

Upon minimization of U and identification of the nontrivial solution $A \neq 0$, the classic formula for the critical buckling force is deduced, $P_{c0} = 4E_0 I\pi^2/L^2$. Here, E_0 is used to represent the

Young's modulus of the material under no magnetic field.

Now let us turn to the case when the column is under a magnetic field. The detailed distribution of magnetic field around a buckled column is complex. Here we will simplify this problem by utilizing the spatial periodicity of the structure. Consider an array of parallel columns, as depicted in Fig. 4. Instead of looking at the local magnetic field around each column, we will focus on the effective permeability of the entire structure upon homogenization. The structure resembles a composite material with transverse isotropy. The direction of the more permeable columns is the principal direction with maximum permeability. When the columns are tilted (e.g. due to buckling), as shown by Fig. 4b, the principal axis rotates and the effective permeability in the vertical direction μ_{eff} decreases. The effective permeability is, in general, a function of the tilting angle θ. For small buckling amplitude, $\theta << 1$, and the effective permeability can always be expanded into a truncated Taylor series of θ: $\mu_{\text{eff}}(\theta) \approx \mu_1(1 - b\theta^2)$, with μ_1 being the reference permeability of the case when all columns are straight and vertical. Here we have utilized the idealization that all columns tilt at the same orientation to simplify the model. Such an idealization is not essential to the Taylor expansion of μ_{eff} as long as b is kept as an unknown parameter.

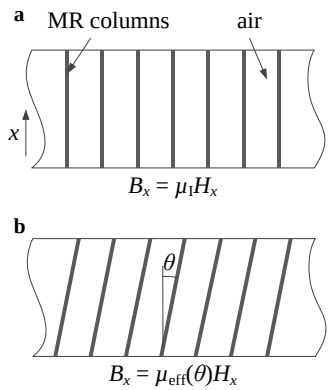

Fig. 4 Sketch of one horizontal thin slice of the MR-brush structure in the (a) reference state, and (b) buckled state. The magnetic behavior of the column-air system resembles that of a composite material.

By treating each section of a buckled column as part of a tilted composite structure with tilting angle $\theta = w'$, we can calculate the magnetic energy per unit cross-sectional area of the brush structure:

$$W_m = \int_0^L \frac{B^2}{2\mu_{\text{eff}}} \mathrm{d}x = \frac{B^2}{2\mu_1}\left(L + 2\pi^2 b \frac{A^2}{L}\right). \quad (4)$$

The total potential energy of the system per unit cross-sectional area is

$$\Pi = \phi U_b + W_m - \sigma\Delta, \quad (5)$$

where ϕ is the number of columns on unit area of substrate. Minimizing Π, we identify the critical condition in which non-zero buckling amplitude A is possible:

$$\sigma_c = 4\phi EI\frac{\pi^2}{L^2} + \frac{bB^2}{\mu_1}. \quad (6)$$

The two terms on the right-hand side of Eq. (6) correspond to the two contributions to the critical stress of an MR brush against buckling: one directly from the material modulus $E(B)$ which increases under a magnetic field, the other from the change in magnetic energy associated with the deformed geometry. Both terms are always positive, giving rise to the amplified stiffening effect of the MR brush. When deriving Eq. (5), we assume the B field to be constant, which approximates the case when the sample is placed in the narrow gap between the opposite poles of two permanent magnets, where the B field is uniform and almost constant. In the case when the magnetic field is applied through electromagnetic coils, the work done by the coil needs to be considered and a similar result shall be obtained.

We can further normalize σ_c by its value in the absence of a magnetic field, $\sigma_{c0} = \phi P_{c0}$, and write the dimensionless critical stress as

$$\tilde{\sigma}_c = \frac{\sigma_c}{\sigma_{c0}} = \tilde{E}(B) + \frac{bB^2L^2}{4\pi^2\phi E_0 I\mu_1}. \quad (7)$$

where $\tilde{E}(B)$ is the dimensionless Young's modulus of the material under magnetic field B: $\tilde{E} = E(B)/E_0$. Having an explicit dependence on various controllable parameters such as B and L, the dimensionless expression (7) could be used to verify the theory developed in this section.

3. Experimental

3.1 Materials and synthesis

The MR brush was developed through the following steps. The polydimethylsiloxane (PDMS) solution and the cross-linking agent (EL P7683/50 A and B, Wacker Chemical Corp.) were mixed with a weight ratio of 1:1, immediately followed by the addition of certain amount of magnetically soft carbonyl iron powder (ISP S-1641, 6 μm average diameter). The mixture was stirred sufficiently to randomly disperse the particles in the polymer solution, and placed in a vacuum chamber for 5 minutes to eliminate bubbles, before poured onto a pre-cured substrate of the same material as the PDMS elastomer matrix. The Petri dish containing the substrate and the mixture was brought into a uniform magnetic field (≤1% spatial variation prior to sample insertion) created by an electromagnet (EMU-75). The magnetic field drove the Rosensweig instability[20] on the free surface of the polymer solution, and further developed a three dimensional columnar structure between the cap of the container and the substrate. The samples were cured under the field for about 3 hours at room temperature, and the columnar structures were solidified on the substrate.

The spatial density of the columnar structure was controlled by the volumetric filling ratio of the polymer-particle mixture, which was kept constant at 25% (the volume of the mixture divided by the volume of the container) throughout all samples. It was found that this filling ratio would yield the most uniform columnar structures. Two groups of samples were prepared by varying the curing magnetic flux density (0.13 T and 0.24 T) and the iron

concentration (33 wt%, 50 wt% and 70 wt%).

3.2 Measurements

Figure 5 shows the micro loading frame built for measuring the mechanical properties of the MR brush samples under various magnetic fields. The axial compressive force was measured by a load cell fixed on the experimental platform. The displacement of the slider was controlled manually and measured through a displacement sensor. A small sample of MR brush was placed between the load cell and the slider, attached either to a permanent magnet or directly to the slider. The readings from the displacement sensor and the load cell were synchronized and collected to establish the force-displacement relationship in each case. All tests were carried out with displacement-controlled loadings, so that the unstable post-buckling behavior can be captured.

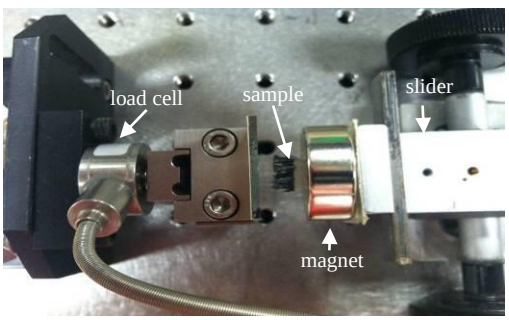

Fig. 5 Experimental setup for measuring the properties of MR brush under magnetic field.

Limited by the working space and more importantly by the range of the field generated by the permanent magnet, only a small portion of MR brush could be tested at each time. To obtain the overall performance of a larger brush structure, it was cut into small pieces and tested individually, and the results were then averaged over six independent measurements. The force data were divided by the substrate area (not the cross-sectional area of the bristles) to obtain the nominal stress.

4. Results and discussion

4.1 Influence of synthesis parameters

Both the morphology and performance of the MR-brush structure are highly dependent on synthesis conditions. In this section, the dependences on two most important parameters, the curing magnetic field and the concentration of filler iron particles, will be presented.

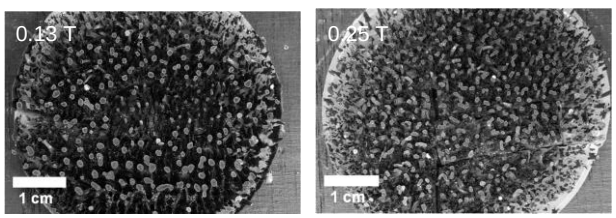

Fig. 6 Top view of the MR-brush samples cured under magnetic field of different strengths as marked.

It is known that in anisotropic MR elastomers, better particle alignment and better performance can be achieved for materials cured under stronger fields.[21] The influence of the curing field strength was found to be similar for MR-brush structures. Generally, a higher field leads to more uniform bristles. Two batches of samples cured under magnetic fields of 0.13 T and 0.25 T were tested and compared. The length of brush bristle measured approximately 4 mm and the iron particles were mixed at a 50% concentration by weight, and the bristle number densities were 0.23±0.02 mm^{-2} and 0.44±0.04 mm^{-2} respectively. The representative structures are shown in Fig. 6. The sample cured at stronger field exhibited more regular column shapes and more uniform distribution. Also stronger curing field tends to yield samples with thinner and thus denser bristles. It is believed that this dependence is due to the competition among magnetic force, gravity, viscous force, and surface tension. A stronger curing field will dominate over all other factors, resulting in well-defined columnar structure of the precursor mixture along the field lines.

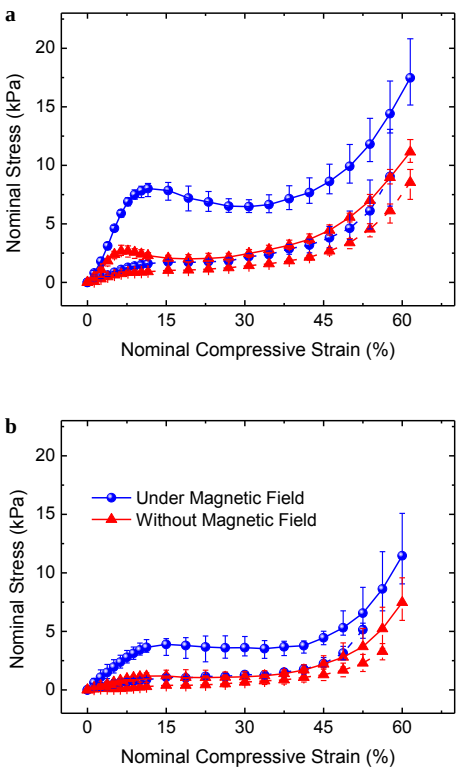

Fig. 7 Measured stress-strain curves of MR-brush samples with different curing magnetic fields at (a) 0.25 T and (b) 0.13 T. Each figure compares the behaviours of a sample under a magnetic field of 0.37 T and without a magnetic field. The solid curves represent the loading cases, and the dash curves indicate the unloading cases. The error bars show the range of data measured from different portions of the same sample.

Shown in Fig. 7 are the typical stress-strain curves of the MR-brush samples. The solid curves represent the loading response, and the dash curves represent unloading. Each loading curve exhibits three stages: the initial linear segment corresponds to the pre-buckling stage in which most bristles are straight, the intermediate plateau in which most bristles buckle, and the final increase stage in which some bristles are severely bent and make

contact with each other or with the substrate. Just as expected, when an external magnetic field (0.37 T) is applied, both the initial stiffness and the critical stress for buckling increase significantly from the corresponding zero-field values. Comparing between Figs. 7a and 7b, it is clear that the sample cured under stronger field had better performance. The stress window for the amplified stiffness change is over 5 kPa for the sample cured at 0.25 T, much larger than the 3 kPa window of the sample cured at 0.13 T.

One should also notice the large hysteresis between the corresponding loading and unloading curves. More interestingly, the hysteresis is much larger under a magnetic field. Because all tests were performed quasi-statically, the influence of viscoelasticity should be minimal. We believe this hysteresis to be originated from the friction between the brush bristles and the punch surface, and that between neighbouring filler particles inside the material. While the former can be reduced by capping the brush structure by another substrate, the latter may not be eliminated. Although this hysteresis causes the effective stiffness to be dependent on the loading history and complicates the design of devices in applications, the large field-dependent hysteresis may give rise to other potential applications of this structure, such as a smart vibration absorber.

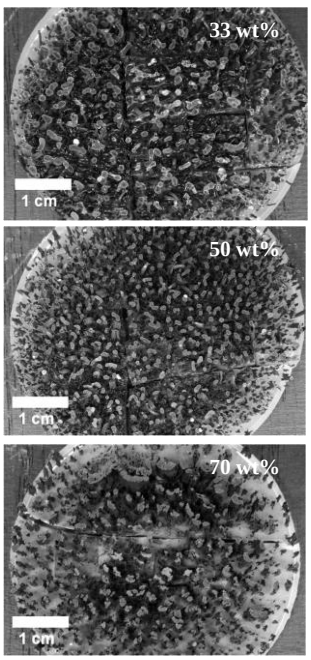

Fig. 8 Top view of the MR-brush structures synthesized with different iron concentrations.

To study the influence of filler-particle concentration, we tested the samples synthesized with three representative concentrations of iron particles: 33 wt%, 50 wt%, and 70 wt%. All samples in this test were cured under a uniform field of 0.25 T. The bristle length for all samples was kept at approximately 4mm, and the number densities were $0.17 \pm 0.02\ \mathrm{mm}^{-2}$, $0.44 \pm 0.04\ \mathrm{mm}^{-2}$ and $0.12 \pm 0.02\ \mathrm{mm}^{-2}$ respectively. It was found that the sample morphology was highly dependent on the filler concentration, as shown by Fig. 8. At a lower filler concentration, the precursor mixture was less viscous and the shape of the columnar structure was not well-controlled by the curing field. As a result, the final structure contained many relatively thin columns that were already bent as synthesized. In the other extreme, if the filler concentration is two high, the high viscosity prevents the magnetic field from spreading the mixture into thinner columns. As observed in the experiments, the mixture agglomerated and formed thick columns, and the distribution appeared to be very non-uniform. At an intermediate filler concentration, ~50 wt%, the resulting brush structure found a balance between column thickness and uniformity. The stress-strain curves of all three compositions, under an applied magnetic field of 0.37 T, are shown in Fig. 9, together with the zero-field stress-strain curves. Compared with the 33 wt% samples, the 50 wt% samples had a much larger window for the amplified MR effect. When the filler concentration was further increased to 70 wt%, the improvement on the critical load is not significant. At the same time, a much larger scattering in the data was observed, due to the deteriorated structural uniformity in the high filler concentration samples. It should also be noted that the optimal filler concentration is also dependent on the strength of the curing field, as well as many other parameters, such as the size of the filler particles. For samples cured under a much higher field, 50 wt% may not be the optimal filler concentration. The detailed parametric study, however, is beyond our current testing capability.

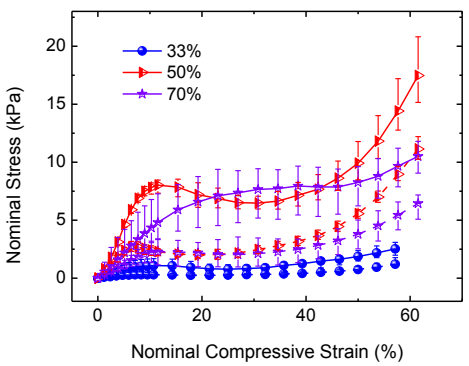

Fig. 9 Measured stress-strain curves of MR-brush samples with different iron particle concentrations. The solid curves show the behavior under a magnetic field of 0.37 T, and the dash curves indicate the zero-field references. The unloading curves are omitted. The error bars show the range of data measured from different portions of the same sample.

4.2 Magnetically tuneable structural stiffness

Finally, to characterize the tuneable stiffness of MR brush, we measured the stress-strain curves of a specific sample under applied magnetic fields of various strengths (0 T ~ 0.37 T). The samples used in this test were cured under a magnetic field of 0.46 T. Each brush bristle measured 5 mm in length and the bristle number density was $0.57 \pm 0.05\ \mathrm{mm}^{-2}$. As shown by Fig. 10a, the loading part of each stress-strain curve can be characterized by two key parameters: the initial slope of the curve, which will be referred to as the initial modulus hereafter, and the turning point of the curve, i.e. the critical stress for buckling. As expected, both the initial modulus and the critical stress increase monotonically with the strength of the applied magnetic field. The tuneable range of stiffness can be extracted from curves like those shown in Fig. 10a by looking at the

intersection between different curves and a horizontal line, which indicates a specific compressive stress. Some values of the effective stiffness (nominal stress divided by nominal strain) were extracted and plotted on Fig. 10b. Clearly, with the application of an external magnetic field, the effective stiffness of the structure is tuneable by up to 20 times. Nevertheless, unlike solid MR elastomers, the stiffness change is dependent on the level of mechanical stress. The structure is the most sensitive when the mechanical load is close to the critical stress under the applied magnetic field. This property suggests that in applications, the strength of the magnetic field may need to be changed dynamically according to the then current load in order to have an optimal sensitivity.

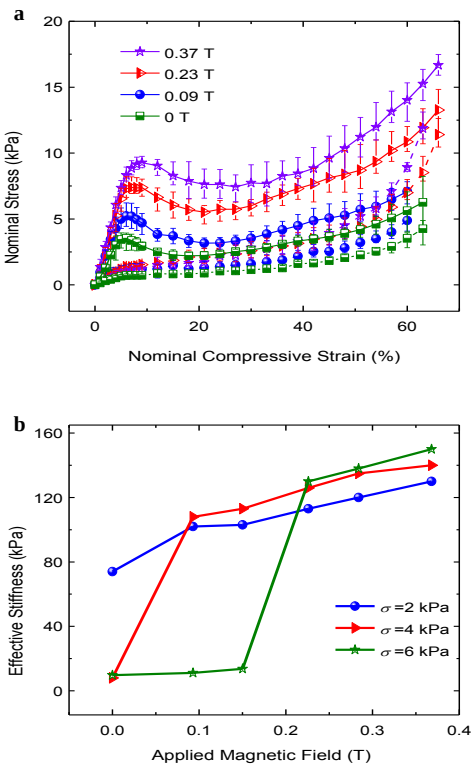

Fig. 10 (a) Measured stress-strain curves of MR-brush samples with different applied magnetic fields. The solid curves represent the loading cases, and the dash curves indicate the unloading cases. (b) The calculated effective stiffness (nominal stress/nominal strain) during loading at different magnetic fields.

It can be seen from Fig. 10a that the increase in the critical stress is more than just the effect of the modulus increase, i.e. the critical strain for buckling is higher under stronger magnetic field. To show this effect explicitly, we extracted the values of the initial modulus and critical stress, and plotted them as functions of the applied magnetic field in Fig. 11a. Just as that of solid MR elastomers,[2,6] the initial modulus of MR brush saturates at a relatively high magnetic field (~0.3 T). On the other hand, the increase in critical buckling stress with magnetic field follows a very different trend. No sign of saturation was observed up to a magnetic field of 0.4 T. This disparity can be explained by the model developed in Section 2. The difference between the critical stress and the initial modulus is extracted from Fig. 11a and plotted in Fig. 11b. It is clear that the normalized difference between the two quantities scales with the squared of the applied magnetic field: $\tilde{\sigma}_c - \tilde{E} \propto B^2$, just as that predicted by the simple model in Section 2, Eq. (7). It is noteworthy that the scaling relation between the buckling stress and applied field is similar to that of MR fluids,[22] and the similarity between the two systems also includes the shape of the stress strain curves. In fact, the arrangement of iron particles in the MR brush is just like the columnar structures of suspensions in a MR fluid. The difference is that a MR fluid does not have the contribution from the modulus $\tilde{E}$.

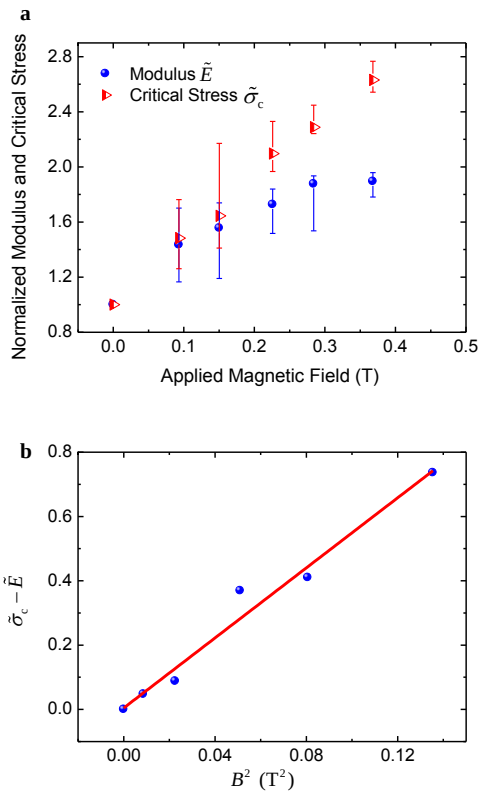

Fig. 11 (a) Dimensionless Young's modulus and critical buckling stress under different applied magnetic fields. (b) Difference between normalized critical buckling stress and modulus. The filled circles are experimental data, and the line is the linear fit as suggested by the model in Eq. (7).

5. Conclusions

Subject to an axial compression beyond a critical value, a solid column buckles. If the column is made of an MR elastomer, the critical load can be significantly increased by applying a magnetic field. There are two contributions to the increase in the critical load: the increase in the modulus of the MR elastomer under the field, and the magnetic field in the environment which favours the more permeable columns as straight pathways along the field direction. A simple buckling instability model is developed in this paper by considering both contributions, and its prediction agrees with experimental observation. The methodology in deriving the buckling model may also be applicable to the analysis of MR fluids, of which the yield stress is related to the critical buckling stress of the MR brush structures

presented here.

Utilizing the tuneable critical load of an MR elastomer column, a soft structure with highly tuneable stiffness, the MR brush, is reported in this paper. By combining the MR effect of the material and the buckling instability, the MR brush is capable of changing its stiffness by up to two orders of magnitude. The dependence of the performance of MR brush on various synthesis parameters has been investigated. It is found that a higher curing field generally yields better results, and an intermediate filler concentration leads to more uniform and well-defined columnar structures. While the columnar brush structure is not necessarily the optimal structural form, the combination of mechanical instability and MR effect suggests a possible way of designing a variety of smart structures with highly tuneable stiffness. Moreover, as the amplification mechanism of buckling is independent of the specific material used, even larger tuneable range can be expected when used in conjunction with emerging new MR materials.

Acknowledgements

This work was supported by the National Science Foundation through a project on magneto-active polymers (CMMI-0900342). XH acknowledges the financial support from Tsinghua University for his visit at Iowa State University. XQF acknowledges the support from the 973 Program of MOST (2012CB934101 and 2013CB933033) and Tsinghua University (20121087991).

[a] *AML and CNMM, Department of Engineering Mechanics, Tsinghua University, Beijing 100084, China*
[b] *Department of Materials Science and Engineering, Iowa State University, Ames, IA 50011, USA*
[c] *Department of Aerospace Engineering, Iowa State University, Ames, IA 50011, USA. Fax: 1-515-294-3262; Tel: 1-515-204-8850; Email: whong@iastate.edu*

References

1. Z. P. Shulman, V. I. Kordonskii, E. A. Zal'tzgendler, I. V. Prokhorov, B. M. Khusid and S. A. Demchuk, *Magnetohydrodynamics*, 1984, **20**, 223.
2. M. R. Jolly, J. D. Carlson, B. C. Muñoz and T. A. Bullions, *J. Intell. Mater. Syst. Struct*., 1996, **7**, 613.
3. M. Zrínyi, L. Barsi and A. Büki, *Polym. Gels Network*, 1997, **5**, 415.
4. T. Takagi, *J. Intell. Mater. Syst. Struct*., 1999, **10**, 575.
5. J. de Vicente, D. J. Klingenberg and R. Hidalgo-Alvarez, *Soft Matter*, 2011,7, 3701.
6. J. M. Ginder, L. C. Davis and L. D. Elie, *Int. J. Mod. Phys. B*, 1996, **10**, 3293.
7. W. H. Li and H. Du, *Int. J. Adv. Manuf. Technol.*, 2003, **21**, 508.
8. H.-J. Jung, B. F. Spencer Jr. and I.-W. Lee, *J. Struct. Eng*., 2003, **129**, 873.
9. M. Brigley, Y.-T. Choi, N. M. Wereley and S.-B. Choi, *J. Intell. Mater. Syst. Struct*., 2007, **18**, 1143.
10. F. D. Goncalves, J. H. Koo, M. Ahmadian, *The Shock and Vibration Digest*, 2006, 38, 203.
11. Z. Varga, G. Filipcsei and M. Zrínyi, *Polymer*, 2006, **47**, 227.
12. X. Wang, F. Gordaninejad, M. Calgar, Y. Liu, J. Sutrisno and A. Fuchs. *J. Mech. Design*, 2009, **131**, 091004.
13. S. A. Demchuk and V. A. Kuz'min, *J. Eng. Phys. Thermophys.*, 2002, **75**, 396.
14. M. Lokander and B. Stenberg, *Polym. Test.*, 2003, **22**, 245.
15. Y. Xu, X. Gong, S. Xuan, W. Zhang and Y. Fan, *Soft Matter*, 2011, **7**, 5246.
16. P. von Lockette, S. E. Lofland, J. Biggs, J. Roche, J. Mineroff and M. Babcock, *Smart Mater. Struct.*, 2011, **20**, 105022.
17. Y. Han, W. Hong and L. E. Faidley, *Int. J. Solids Struct.*, 2013, 50, 2281.
18. H. An, S. J. Picken and E. Mendes, *Soft Matter*, 2010, **6**, 4497.
19. T. Mitsumata, A. Honda, H. Kanazawa, and M. Kawai, *J. Phys. Chem. B*, 2012, **116**, 12341.
20. R. E. Rosensweig, *Ferrohydrodynamics*, Cambridge University Press, Cambridge, 1993.
21. A. Boczkowska, S. F. Awietjan and R. Wroblewski. *Smart Mater. Struct*., 2007, **16**, 1924.
22. R. Rosensweig, *J. Rheol., 1995*, **39**, 179.